Hard X-ray emission of the microquasar GRO J1655−40 during the rise of its 2005 outburst.

A. Joinet[1], E. Kalemci[2], F. Senziani[3,4,5]

ABSTRACT

We present the analysis of the high energy emission of the Galactic black hole GRO J1655−40 at the beginning of its 2005 outburst. The data from 458 ks of *INTEGRAL* observations, spread over 4 weeks, are analyzed, along with the existing simultaneous *RXTE* and *Swift* data. The high energy data allow us to detect the presence of a high energy cut-off and to study its evolution during the outburst rise. This high energy feature is generally related to thermal mechanisms in the framework of Comptonization models from which we can estimate the plasma parameters. We found an electron temperature of about 30-40 keV and an optical depth around 1.8-2.1. The high energy cut-off decreased along with the radio flux, and disappeared as the jet turned off.

Subject headings: stars: individual: GRO J1655−40 - gamma rays : observations - black hole physics - accretion, accretion disk - X-rays : Binaries

1. Introduction

GRO J1655−40 is a transient Galactic X-ray binary. Since its discovery on July 27, 1994 with BATSE (Zhang et al. 1994) on-board the Compton Gamma-ray Observatory (CGRO), the source underwent several outbursts (i.e. : in 1995 see Zhang et al. 1997, in 1996/1997 see Kuulkers et al. 2000 and Méndez et al. 1998). It is likely to be a low mass X-ray binary and the compact object in this system is probably a black hole (Bailyn et al. 1995) with a mass

[1]CESR, 9 Avenue du Colonel Roche, BP4346, 31028 Toulouse, France

[2]Sabancı University, Orhanlı - Tuzla, İstanbul, 34956, Turkey

[3]INAF-IASF Milano, via Bassini 15, 20133 Milano, Italy

[4]Université Paul Sabatier, 31062 Toulouse, France

[5]Universitá degli Studi di Pavia, Dipartimento di Fisica Nucleare e Teorica, via Bassi 6, 27100 Pavia, Italy

estimated at 6.3 $M_\odot$ (Greene et al. 2001) and a distance of 3.2 kpc (Hjellming & Rupen, 1995) from which we based the calculation of the Eddington Luminosity L_{edd} of the source. A recent work by Foellmi et al. (2006) places an upper limit of 1.7 kpc to the distance, but this upper limit is still under debate. Radio jets were discovered in the mid-1990s and revealed apparent superluminal motion in opposite directions (Tingay et al. 1995).

A transient galactic black hole usually exhibits a complex spectro-temporal variability with the variation of the accretion rate. The changes in their properties allow to characterise the state of the source (see McClintock & Remillard 2006, for a complete description). In the High Soft State (hereafter HSS), the soft X-ray emission dominates the spectrum in the form of a blackbody component which is due to the thermal component from a standard accretion disk. In the Low Hard State (hereafter LHS), the source is characterised by a relatively low flux in the soft X-rays ($\lesssim$ 1 keV) and a high flux in the hard X-rays ($\sim$100 keV). *This* is usually interpreted (e.g. Shapiro et al. 1976, Narayan & Yi 1995) as the Comptonization of the soft X-ray photons emitted a cold, geometrically thin disk (Shakura & Sunyaev 1973) by a hot plasma surrounding this accretion disk. The hard component is generally described by a power-law with a photon index of 1.4-1.8, and an exponential cutoff around 100-200 keV. In addition, a Fe Kα line at $\sim$ 6.4 keV and a Compton reflection bump peaking at $\sim$ 30 keV may exist. These are signatures of the irradiation of the cold optically thick disk by the hard X-rays from the corona (George & Fabian 1991). The LHS is characterized by radio emission which has been shown to be consistent with a midly relativistic (v $\simeq$ 0.6c) jet (Gallo et al. 2003). Before entering into the HSS, the source may go through transitional states also called intermediate states. Homan & Belloni (2005) divides the intermediate state into the hard intermediate state (HIMS) and the soft intermediate state (SIMS) which depend on the power density spectra and the spectral index. The jet starts to be quenched *in* the intermediate state (e.g. Corbel et al. 2004).

We present here an analysis of the spectral evolution of GRO J1655−40 during the rising phase of the 2005 outburst. The analysis is based on the data taken by the International Gamma-ray Laboratory (*INTEGRAL*; Winkler et al. 2003). GRO J1655-40 has been observed by *INTEGRAL* starting from MJD 53425 (*INTEGRAL* revolution 289 on 2005 February 24) to MJD 53448 (*INTEGRAL* revolution 296 on 2005 March 19). The spectral and timing evolution of the source from the Proportional Counting Array (*P*CA) on board the Rossi X-ray Timing Explorer (*RXTE*) in the 3-30 keV energy range has been studied in detail in Shaposhnikov et al. 2007 from MJD 53419 up to MJD 53445. Brocksopp et al. 2006 presented the data from the Burst Alert Telescope (*BAT*) on board the *Swift* observatory in the 14-150 keV energy range from MJD 53430 up to MJD 53435. Caballero-Garcia et al. (2007) presented the results of the analysis of 4 ToO observations from 27 February to 11 April of 2005 using JEM-X, ISGRI, and SPI onboard the INTEGRAL observatory and

interpreted it in the framework of several physical models. They come to the conclusion that no cut-off is necessary to describe the data in the LHS.

We studied the broadband spectral evolution using the Spectrometer on board the *INTEGRAL* (SPI, Vedrenne et al. 2003) in the 23-600 keV energy range combined with all the publicly available data from the PCA and HEXTE detectors on board the RXTE observatory, as well as the BAT detector in order to cover the 3-200 keV energy range. One of the main interest in studying such a source during the LHS to the HSS transition is to follow the evolution of the high energy cutoff. We propose to quantify its value as well as its significance during the rising phase of the outburst.

We briefly describe the data analysis methods for *INTEGRAL* (SPI), *RXTE* (PCA and HEXTE), and *SWIFT* (BAT) in Section 2. The scientific results from the spectral modelling are presented in Section 3.

2. Observations and data reduction

GRO J1655−40 started a new outburst on February 17, 2005 (MJD 53418) observed by Markwardt & Swank (2005) with the PCA detector onboard the *RXTE* observatory. This reactivation was confirmed by Torres et al. 2005 who reported the near infrared activity of the source on Februay 21, 2005. *INTEGRAL performed follow-up observations on GRO J1655-40 starting at MJD 53425.* Table 1 gives the details of each *INTEGRAL* revolution and corresponding quasi simultaneous *RXTE* observations used in this analysis.

2.1. *INTEGRAL* data reduction

The data from the SPI detector were reduced as explained in Joinet et al. 2005 except that only 17 detectors were active *compared to 19 in the beginning of the mission.* The SPIROS V6 algorithm has been used in order to derive the position of sources detected in the field of view of GRO J1655-40. We refer to Joinet et al. 2005 (section 2.1.1) for the method of the spectral reconstruction. Only pointings for which GRO J1655−40 was at a distance less than 12 degrees from the central axis were taken into account for the analysis. We excluded pointings affected by a solar flare or by exit/entry into the radiation belts. We obtained 458 ks of useful data during the observation period covered by the revolutions 289 up to 296 (see Table 1). *Revolutions 295 & 296 have been merged and will be named 295,6.* The variability time scale of each source was estimated (see section 3.1) on the basis of both their intensity and their known temporal behavior. The background flux is stable within

each of the considered revolution except for revolutions 292 and 293 for which a variability time scale of one pointing (with a duration of 30-40 minutes) was used. We consider only one normalization parameter per orbit with an uniformity map determined for the 17 detectors configuration.

We limited the energy range from 23 to 600 keV for the SPI data and added a 3 % systematic error to all spectral channels. *The ISGRI data corresponding to revolutions 290, 295 & 296 which was published in Cabarello-Garcia et al. 2007, has also been included for the analysis.*

2.2. *RXTE* data reduction

We also analyzed the public data from the PCA and HEXTE detectors on board the *RXTE* observatory (Bradt et al. 1993, Rothschild et al. 1998) data. Table 1 summarizes the set of *RXTE* observations performed contemporaneously with the *INTEGRAL* data observation periods except for the revolution 294 for which there *are* no INTEGRAL data available. This observation period has been divided into three. Several RXTE observations have been merged in order to correspond to one integrated *INTEGRAL* revolution.

For both instruments the data reduction *were* performed using the FTOOLS routines in the HEAsoft software package distributed by NASA's HEASARC (version 6.0.4).

All available PCUs of the PCA (Bradt et al. 1993) detector have been used for the data extraction. We added 0.8% up to 7 keV and 0.4% above 7 keV as systematic error (Tomsick et al. 2001)

For HEXTE, we used the response matrix created by the FTOOLS, and applied the necessary dead time correction (Rothschild et al. 1998). The HEXTE background is measured throughout the observation by alternating between the source and background fields every 32 s. The data from the background regions are merged.

We limited the energy range from 3 to 25 keV, and 16 to 227 keV for the PCA and HEXTE data, respectively. *HEXTE* channels were grouped by 2 for channels 16-31, by 4 for channels 32-59, by 10 for channels 60-99 and by 64 for channels 100-227.

2.3. *Swift* data reduction

All the publicly available data from the BAT detector on board the *Swift* observatory (Gehrels et al. 2004 , Barthelmy et al. 2005) covering the rising phase of the 2005 outburst

were also analysed (see Table 2). Some of them were simultaneous with the *INTEGRAL* revolutions (292, *295,6*). The revolution 292 has been divided into two datasets *composed of 7 BAT pointings* with a duration of 10.09 ks for 292_{sw}-A, and 7.66 ks for 292_{sw}-B. We also used the *Swift* data covering the observation period between the INTEGRAL revolutions 292 and 293 (293_{sw}) and between revolutions 293 and 295-B ($294_{sw} - A$ and $294_{sw} - B$). We reduced the data using the standard *Swift* software[1] (version 2.4). A standard filtering was applied in order to discard the data affected by high background rate and source occultations. For each interval over which the BAT pointings were unchanged, we extract a background subtracted spectra together with the response matrix using the mask-weighting technique. Systematic errors were applied to the spectra using *batphasyserr* BAT FTOOL. For the spectral analysis, we limited the energy range from 16 to 150 keV.

For both the *RXTE* instruments and the BAT, the normalization factor was set free with respect to SPI normalization for all fits.

3. Results

3.1. Light curve

The flux extraction of GRO J1655−40 from SPI observations was performed taking into account the hard X-ray sources detected in the field of view of the source. We used a timescale of one pointing (whose duration is about 3600 s) for 4U1700-377 and OAO 1657-415 and two pointings for GX 340+0 and 4U 1705-322. We also considered other sources (GRO J1655−40, 1E 1740-2942, 4U 1630-47, GX337+00 and GX349+2) with a constant flux within each revolution. As the significance of sources decreases above 150 keV, we considered only two sources with a timescale resolution of 3600 s for 4U1700-77, and one revolution for GRO J1655−40, to extract fluxes in the 150-600 keV energy range. The light curve of the source from revolution 289 up to revolution 296 in the 23-51 keV energy range is shown in Figure 1. As the source was in the border of the SPI field of view between INTEGRAL revolutions 293 and 295-B, we used the *RXTE* and the BAT observations (294_{sw}-A, 294_{sw}-B) to *cover this period.* Table 3 gives the SPI and BAT fluxes in different energy bands.

We also extracted the light curve obtained by the *RXTE* all-sky monitor ASM in the 1.5-12 keV energy range in the same period (data taken from the public XTE database[2]). The different states harbored by the source were determined by Shaposhnikov et al. 2007

[1] *http://swift.gsfc.nasa.gov/docs/software/lheasoft*

[2] http://xte.mit.edu/lcextrct/asmsel.html

on the basis of the X-ray properties from the PCA observations and are summarized in Figure 1. The source was in the LHS from revolution 289 up to revolution 292, it then entered the HIMS from revolution 293 (also observed by the BAT detector : datasets 293_{sw} and 294_{sw}-A), the SIMS during the revolution 294-A and was in the HSS from revolution 295-A. Revolution 294 has been divided into three RXTE datasets (294-A, 294-B and 294-C) in order to follow the evolution of the high energy cutoff during the SIMS.

As seen from the SPI light curve (Figure 1), the 23-51 keV flux increased by a factor of 2.5 between MJD 53425 (42 ± 2 mCrab) and MJD 53433 (121 ± 7 mCrab) while the source was in the LHS. A radio ejection was observed between MJD 53429-53433 with a radio peak at 5 GHz (Shaposhnikov et al. 2007). After this ejection, the X and γ-ray flux increased exponentially up to *INTEGRAL* revolution 293 or MJD 53437-53438 (280 ± 7 mCrab) during which the source was into the HIMS. As the flux in the 3-25 keV energy range measured from PCA data increased by a factor 3.9, the flux in the 23-51 keV energy range decreased by a factor *3.5* between revolution 293 and revolution $295{,}6_{sw}$ indicating the LHS to the HSS transition.

3.2. Spectral Modeling of the X and γ-ray data

The spectra corresponding to each set of data in Table 1 and 2 have been fitted with various models available in the standard XSPEC 11.3.1 fitting package (Arnaud 1996). In all fits, the iron emission line was modelled by a narrow Gaussian line fixed at an energy of 6.4 keV with a free width. For all models, the inner disk inclination was fixed at 70° (Van de Hooft et al. 1998). We also consider the emission from a multicolor disk blackbody (DISKBB in XSPEC, Mitsuda et al. 1984). We account for the interstellar absorption (PHABS in XSPEC) *using a hydrogen column density N_H of 0.7 for most of the observations (see § 3.2.1 for exceptions)* which is based on the values constrained by XMM-Newton observation during the 2005 outburst (Diaz Trigo et al. 2007).

3.2.1. Power law with a cutoff

First, a power-law component is added to the base model described above. The best fit parameters are presented in Table 4. During the LHS (revolutions 289, 290, 291, 292), we found a constant spectral index Γ of $\simeq 1.47$ (with a reduced χ^2 ranging from 1.7 up to 2.0).

During revolutions 289, 290 and 291, the fits are significantly improved, as seen from the reduced χ^2 values, (with an F-test probability less than 10^{-9}) by adding a high energy cutoff

component (see Table 4). A constant spectral index Γ of about 1.33-1.36 has been obtained, which is almost the *same* value found by Shaposhnikov et al. 2007 (1.35 ± 0.03). The high energy cutoff of 231^{+94}_{-50} keV is consistent with the range value of 163-214 keV presented in Shaposhnikov et al. 2007 for the revolution 289. The SPI data that we analyzed for all the outburst allow to constrain its value and to precisely describe its evolution which has not been done in Shaposhnikov et al. 2007. *However we reach a conclusion contrary to Caballero-Garcia et al. 2007 which show that no cutoff was required to describe the data corresponding to revolution 290. We fit the dataset corresponding to the revolution 290 using PCA, ISGRI and SPI data with the following model : PHABS(DISKBB+POWERLAW)HIGHECUT in order to compare our results with the ones of the reference Caballero-Garcia et al. (2007). We found a high energy cut-off powerlaw constrained to a value of* 22^{+6}_{-8} *keV and a folding energy of* 193^{+14}_{-21} *keV with a reduced* χ^2 *of 0.83 (87 degrees of freedom or dof). By fitting ISGRI and PCA then SPI and PCA, we found a folding energy of* 193^{+27}_{-22} *keV (with a reduced* χ^2 *of 0.79 (71 dof)) and* 201^{+91}_{-92} *keV (with a reduced* χ^2 *of 0.65 (56 dof)), respectively. By fitting ISGRI, HEXTE and PCA data, we found a folding energy of* 253^{+34}_{-31} *keV and a photon index of* $1.40^{+0.02}_{-0.02}$ *(with a* χ^2 *of 1.43 (90 dof)).*

For revolution 292, E_c is constrained to a value of 187^{+22}_{-20} keV. BAT data *were* combined with the simultaneous PCA, HEXTE and SPI data corresponding to the *INTEGRAL* revolution 292 in order to check the cross calibration between all instruments. During revolutions 289-292, the disc component was very weak.

We then notice a decrease of E_c down to 87^{+4}_{-5} keV during revolution 294a as the source is into the HIMS (Shaposhnikov et al. 2007). The disc component also got stronger, while the power law index remained relatively constant.

By fitting simultaneously BAT, PCA and HEXTE data for revolution 294 (datasets 294-B and 294_{sw}*-B), when the source has entered the SIMS, a pure powerlaw results in a reduced* χ^2 *of 1.16 (118 dof). Adding a high-energy cutoff results in significant reduction in reduced* χ^2 *(0.99, 117 dof) but the folding energy is not constraining (*302^{+225}_{-81} *keV), and strongly depends on the power-law index.* The disk component also starts to dominate the energy spectrum as shown from the clear changes in the Φ_p/Φ_b ratio (Table 4) (where ϕ_p is the powerlaw flux and ϕ_b the blackbody flux in the 2-20 keV energy range). This ratio decreases by a factor 12.93 between revolution 293 and 294-B due to a large increase (by a factor 21) of the disk component Φ_b. The contribution of the hard component with respect to the disk component is lower than 50% during revolution 294-B. Moreover, the photon index becomes steeper with $\Gamma \simeq 2.1$, indicating a spectral transition.

From the dataset 294-C for which only PCA and HEXTE data are available, there is no evidence of a high-energy cutoff up to 286 keV.

The reduced χ^2 decreases from 2.00(61 dof) down to 1.81(61 dof) and from 1.66(62 dof) down to 1.40(62 dof) for the datasets 294-C and 295-A, respectively, using N_H of 0.5×10^{22} cm^{-2}. The high reduced χ^2 is due to poor modeling of the low energy part of the spectra. A complex spectral feature around 7 keV has been fitted by Diaz Trigo et al. 2007, using XMM-Newton and *INTEGRAL* data.

The spectra corresponding to these fit parameters (Table 4) are shown in Figure 2 and 3.

3.2.2. Reflection model PEXRAV

We fitted all data with a reflection model, PEXRAV in XSPEC (Magdziarz & Zdziarski 1995), consisting of a power-law with a high energy cut-off and reflection from neutral medium (see Table 5). During the LHS, as the luminosity in the 3-600 keV energy range increased by a factor $\simeq 2.8$ from revolution 289 up to revolution 292, the spectral index Γ is constant ($\simeq$ 1.3-1.4). Similar values of the spectral index and of the high energy cutoff are found using the CUTOFFPL and the PEXRAV models: it is explained by the fact that the reflection fraction is so low that an additional reflection component is not required in the fit. *The range of values for the high energy cutoff (180-380 keV) are consistent with the results of Shaposhnikov et al. 2007 (*196 ± 48 *keV) for the revolution 289. We determine an upper limit on the energy cutoff when the source is into the HSS :* $E_c > 2000$ *keV for the datasets 295,6 + 295,6$_{sw}$ (see Table 5).*

During all observations (from the LHS to the HSS), the reflection component *is not constrained* and do not exceed 0.2, which is lower than the values found in Shaposhnikov et al. 2007 ($\Omega \simeq 0.5$).

3.2.3. Comptonization model COMPTT

The hard power law plus cut-off spectrum of the LHS is usually interpreted as thermal Comptonisation in a hot (kTe$\sim$ 100 keV) optically thin plasma (the corona). We used COMPTT model (Titarchuk 1994) in order to describe this high energy process. The temperature of the disk (T_{in}) in the multicolor disk blackbody model is forced to be equal to the soft photon temperature (T_0) of the Comptonization model. We see in Table 6 that the optical depth is $\simeq 1.8 - 2.0$ while the temperature decreases from $\simeq 40$ down to $\simeq 30$ keV from the LHS to the HIMS. By freezing the temperature to 37 keV which is the value obtained by Shaposhnikov et al. 2007 for the dataset corresponding to the *INTEGRAL* revolution 289, we determined an optical depth of $1.98^{+0.05}_{-0.05}$ which is lower by a factor 2.2 compared to the

value found in this reference. Moreover the inner disk temperature is higher : $T_{in} = 0.83$ keV instead of 0.60 keV. That could be explained by the fact that the continuum above 100 keV constrained with the *INTEGRAL* data is different in this reference.

Regardless of the fit models, we can describe the spectral evolution in terms of an evolution of the geometry based on the Compton parameter $y = 4kT/m_ec^2\ max(\tau, \tau^2)$ (where the electronic temperature kT and the optical depth τ are derived from a Comptonization model, Sunyaev & Titarchuk, 1980). *During the LHS, the Compton parameter is not varying significantly ($y \simeq 0.6$). It starts to decrease from the HIMS (revolution 293), and is correlated with the increase of the normalization of the disk component. It decreases (see value in Table 6) by a factor 4.3 between revolution 289 and revolution 294-B when the source is into the SIMS.* The LHS to the Intermediate state (both HIMS and SIMS) transition corresponds to a gradual decrease of the inner radius of the cold accretion disk, associated with either the cold disk penetrating the hot inner flow, or the latter collapsing into an optically thick accretion disk with small active regions of hot plasma on top of it (Zdziarski et al. 2002). The enhanced soft photon flux from the disk tends to cool down the hot phase, leading to softer spectra. This can be directly observed from the evolution of the blackbody component with respect to the powerlaw component (see the ratio Φ_p/Φ_b given in Table 4).

4. Discussion

4.1. High energy cutoff and jet quenching

We determined that all datasets in the low hard state requires a high energy cut-off. In addition to F-tests that indicate that the cut-offs are required, we have produced contour plots of cut-off versus power-law index for each dataset and those also substantiated the existence of the cut-off in single revolutions. In Figure 5, the contour plot corresponding to the revolution 290 clearly shows the requirement of the high energy cutoff during this observation period which has also been studied in the reference Caballero-Garcia et al. 2007. However, those last ones deduced that no cutoff was required for this dataset. These results are not compatible with those found by Caballero-Garcia et al. (2007) using JEM-X, ISGRI and SPI data who deduced that no energy cutoff was required. The main difference between our analysis and theirs is the fact that we have used the PCA to constrain the low energy part of the spectrum whereas in Cabarello et al. JEM-X has been used.

For PEXRAV and CUTOFF models, the data from datasets 294-B and 294-C indicate that either the high energy cutoff increases significantly, or the cutoff vanishes completely. Such evolution was observed for GX339-4 in the HIMS (Belloni et al. 2005), and now

appeared in the SIMS in the case of GRO J1655-40.

We attempt to describe this high energy feature by adding a powerlaw component to the Comptonization model COMPTT. We found that the addition of a power-law component leads to an improvement of the fit significant at the 99.9998% level for both datasets according to a F-test, with a best fit *photon* index Γ of $3.86^{+0.12}_{-0.18}$ and $3.95^{+0.40}_{-0.35}$, respectively. The powerlaw component contributes at 23% and 20% of the 2-20 keV flux for the revolution 294-B and 294-C, respectively. The extension of a powerlaw at high energy has already been observed in the Steep Power Law State of GROJ1655-40 during its 1996 outburst (see Remillard & McClintock 2006). It is interpreted as inverse Compton scattering that occurs in a non-thermal corona, which may be a simple slab operating on seed photons from the underlying disk (Zdziarski et al. 2005). The origin of the Comptonizing electrons is still a subject of debate. Poutanen & Fabian (1999) *suggested* that flare regions erupting from magnetic instabilities in the accretion disk could explain such a Comptonizing media. The association of a non-thermal process with a state transition has also been discussed for Cyg X-1 (Malzac et al. 2006), in this case interpreting the power-law tail as the Comptonization of soft photons by accelerated electrons (see also Titarchuk 1997). Finally, such a high energy emission could also come from an optically thick electron-positron outflow covering the whole inner region of the accretion disk (Beloborodov 1999b).

As seen from the Figure 4, there is a correlation between the radio intensity and the exponential energy cutoff. The maximum flux in radio is achieved when the source is in the LHS. When the source *enters* the HIMS, the high energy cut-off decreases (or the plasma cools down) as well as the radio flux. Quenching of the jet in the soft states of black hole binaries is known for many sources (Fender et al. 1999, Corbel et al. 2000). Here we show a clear evolutionary path to this quenching in terms of plasma temperature, perhaps associated with the cooling and shrinking of the corona.

4.2. The jet ejection event

The jet ejections usually *occur* at or near state transitions prior to the source entering the IS (Corbel et al. 2004). A radio flare ejection is observed for GRO J1655-40 during the revolution 291, just before the X- and γ-ray flux peak. Such a behavior has also been observed for the black hole candidate H1743-322 and GX339-4 (Joinet et al. 2005, Corbel et al. 2000, Fender et al. 1999) and could be linked to a coronal ejection event. The decrease of the Compton y-parameter (see Table 6), and the appearance of the non thermal component (addition of the powerlaw component) indicate large changes in the corona geometry.

Moreover, the small reflection fraction combined with a high coronal temperature (or high energy cutoff) can be explained by the model of Beloborodov (1999a) which argues that the corona above the accretion disk is fed by magnetic flares or by a corona with non-static or outflowing coronae (Malzac et al. 2001). GRO J1655-40 started to enter the IS from the end of the revolution 292. *This* state corresponds to the decay of the radio emission (Figure 4) which is usually dominated by the decaying optically thin synchrotron emission from the jet ejections. During this state, such an emission is decoupled from the black hole system as the emitting electrons are far from it. The radio emission is completely quenched *starting* from the SIMS (revolution 294-B).

5. Conclusion

We clearly observed a transition from the LHS to the HSS during the rising phase of the 2005 outburst of GRO J1655-40 between MJD 53425 and MJD 53445. The outburst was covered with SPI, HEXTE, PCA and BAT which allowed us to determine the high energy cutoff with a high precision. During revolution 294, only data from the *RXTE* and *Swift* observatory were available to constrain the high energy cutoff during an intermediate state. An evolution of the high energy feature was noticed during the LHS : it decreased from a value above 200 keV down to 130 keV when the source reached the maximum of luminosity in the γ-ray domain (above 23-600 keV). During the HSS, an upper limit on the high energy cutoff has been determined. However, based on the decreasing trend of the cutoff energy, and also decreasing hardness of the spectrum, it is more natural to interpret the non-detection as disappearance of the cutoff, rather than a much higher cutoff energy than the detectors could detect. This decrease corresponds to a decrease in the radio flux, and the cut-off disappeared along with the radio jet. Finally, we also discussed on the relation between state transition and the emission of jet in X-ray binaries which is a subjet of large investigation in order to have a complete view of the X-ray geometry. It would be interesting to perform a broadband spectral fitting (from radio up to MeV) in order to discriminate the different non thermal processes suggested in *this* study.

The SPI project has been completed under the responsibility and leadership of the CNES. We are grateful to ASI, CEA, DLR, ESA, INTA, NASA and OSTC for support. Specific softwares used for this work have been developed by L. Bouchet. A. J. thanks N. Shaposhnikov and M. Rupen for all informations concerning the radio detection and M.D. Caballero-Garcia who provided the ISGRI data used in this paper. E. K. acknowledges support of TUBİTAK Career Program 106T570, Turkish National Academy of Sciences Young and Successful Scientist Award and Marie Curie International Reintegration Grant

MIRG-CT-2005-017203.

REFERENCES

Arnaud K. A. 1996, in ASP Conf. Ser., Vol. 101, Astronomical Data Analysis Software and Systems V, ed. G. H. Jacoby, J. Barnes J. (San Francisco: ASP), 17

Bailyn, C. et al., 1995, Nature, 374, 701

Barthelmy, S., et al., 2005, Space Sci. Rev., 120, 143

Belloni, T., Homan, J., Casella, P., van der Klis, M., Nespoli, E., Lewin, W. H. G., Miller, J. M., Méndez, M., 2005, A&A, 440, 207

Beloborodov, A.M., 1999a, ApJ, 510, L123

Beloborodov, A.M., 1999b, MNRAS, 305, 181

Bradt, H.V., Rothschild, R.E., & Swank, J.H. 1993, A&AS, 97, 355

Brocksopp, C., et al., 2006, MNRAS, 365, 1203

Caballero-Garcia, M. D., et al., 2007, ApJ, in press (astro-ph/0706.1302)

Corbel, S., Fender, R. P., Tzioumis, A. K., Nowak, M., McIntyre, V., Durouchoux, P., Sood, R., 2000, A&A, 359, 251,

Corbel, S., Fender, R. P., Tomsick, J. A., Tzioumis, A. K., Tingay, S., 2004, ApJ, 617, 1272

Diaz Trigo, M., Parmar, A. N. , Miller, J.,Kuulkers, E., & Caballero-Garcia, M. D.,2007, A&A, 462, 657

Gallo, E., Fender, R. P., & Pooley, G. G., 2003, MNRAS, 344, 60, 72

Gehrels, N., et al., 2004 , ApJ, 611, 1005

George, I. M., Fabian, A. C., 1991 , MNRAS, 249, 352

Greene, J., Bailyn, C. D., Orosz, J. A., 2001, ApJ

Grove, J. E., Johnson, W. N., Kroeger, R. A., McNaron-Brown, K., & Skibo, J. G., 1998, ApJ, 500, 899

Fender, R., et al., 1999 , ApJ, 519, 165

Foellmi, C., Depagne, E., Dall, T. H., & Mirabel, I. F., 2006 , A&A, 457, 249

Gallo, E., Fender, R. P., & Pooley, G. G., 2003, MNRAS, 344, 60, 72

Greene, J., Bailyn, C. D., Orosz, J. A., 2001, ApJ, 554, 1290

Homan J., & Belloni T., 2005, Ap&SS, 300, 107

Hjellming R. M., & Rupen, M. P., 1995, Nature, 375, 464

Joinet A., et al. 2005, ApJ, 629, 1008

Kuulkers, E., et al., 2000, A&A, 358, 993

Magdziarz, P., & Zdziarski, A. A. 1995, MNRAS, 273, 837

Malzac, J., Beloborodov, A. M., Poutanen, J., 2001, MNRAS, 326, 417

Malzac, J., et al. 2006, A&A, 448, 1125

Markwardt, C. B., & Swank, J., 2005, Atel, 415, 1

McConnell, M. L., et al. 2000, ApJ, 543, 928

McConnell, M. L., et al. 2002, ApJ, 572, 984

McClintock, J.E., & Remillard, R.A. 2006, in Compact Stellar X-ray Sources, ed. W.H.G. Lewin & M. van der Klis (Cambridge: Cambridge University Press), p157

Méndez, M., Belloni, T. &, van der Klis, M., 1998, ApJ, 499, 187

Mitsuda, K., Inoue, H., Koyama, K., et al., 1984, PASJ, 36, 741

Narayan, R., & Yi, I., 1995, ApJ, 452, 710

Poutanen, J., Fabian, A. C. 1999, MNRAS, 306, 31

Remillard , R. A.,& McClintock, J.E., 2006, ARAA, 44,49

Rothschild, R. E., et al. 1998, ApJ, 496, 538

Shakura, N. I, Sunyaev, R. A., 1973, A&A, 24, 337

Shapiro, S.L., Lightman A.P., & Eardley, D. M., 1976, ApJ, 204, 196

Shaposhnikov, N. , Swank, J., Shrader, C.R., Rupen, M., Beckmann, V., Markwardt, C.B., Smith, D.A., 2007, ApJ, 655, 434

Sunyaev, R., & Titarchuk, L., 1980, A&A, 86, 121

Tingay, S. J., et al., 1995, Nature, 374, 141

Titarchuk, L. 1994, ApJ, 434, 570

Titarchuk, L., 1997, ApJ, 487, 834

Tomsick, J. A., Corbel, S. & Kaaret, P. 2001, ApJ, 563, 229

Torres, M. A. P., Steeghs, D., Jonker, P. & Martini, P., 2005, Atel, 417, 1

Van de Hooft, F., Heemskerk, M. H. M., Alberts, F., & van Paradijs, J., 1998 , A& A, 329, 538

Vedrenne, G., et al. 2003, A&A, 411, L63

Winkler, C., et al. 2003, A&A, 411,1

Zhang, S. H., et al., 1994, IAUC, 6106

Zhang, S. N., Ebisawa, K., Sunyaev, R., Ueda, Y., Harmon, B. A., Sazonov, S., Fishman, G. J., Inoue, H., Paciesas, W. S., & Takahashi, T., 1997, ApJ, 479, 381

Zdziarski, A. A., Poutanen, J., Paciesas, W, S., Paciesas, W.S.,& Wen, L., 2002, ApJ, 578, 357

Zdziarski, A. A., et al., 2005, MNRAS, 360, 825

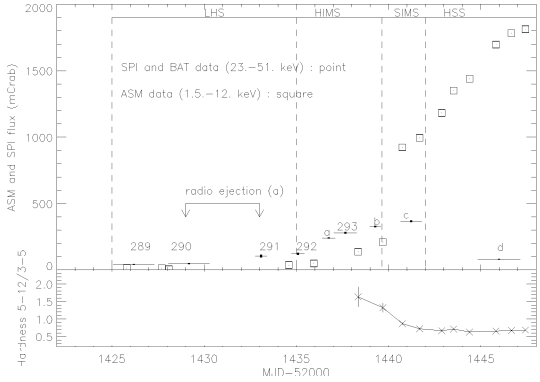

Fig. 1.— Upper panel : ASM (1.5-12 keV), SPI (23-51 keV) light curves of GRO J1655−40 during *the rising phase* of the 2005 outburst. The legend of letters are: a=293_{sw}, b=294_{sw}-A,c=294_{sw}-B, d=295_{sw}, e=296_{sw} . The flux of points a,b,c,d,e has been extracted from BAT observations. The different states harbored by the source are summarized on the graph (see text for the definition): LHS=Low Hard State, HIMS= Hard Intermediate State, SIMS = Soft Intermediate State, HSS=High Soft State. Lower panel : the evolution of the hardness from ASM in the 3-12 keV energy range which is defined as the ratio of the ASM fluxes Φ in two energy ranges Φ [5.-12. keV]/Φ [3.-5. keV]. Two arrows indicate (a) the period associated to a radio flare event (see text).

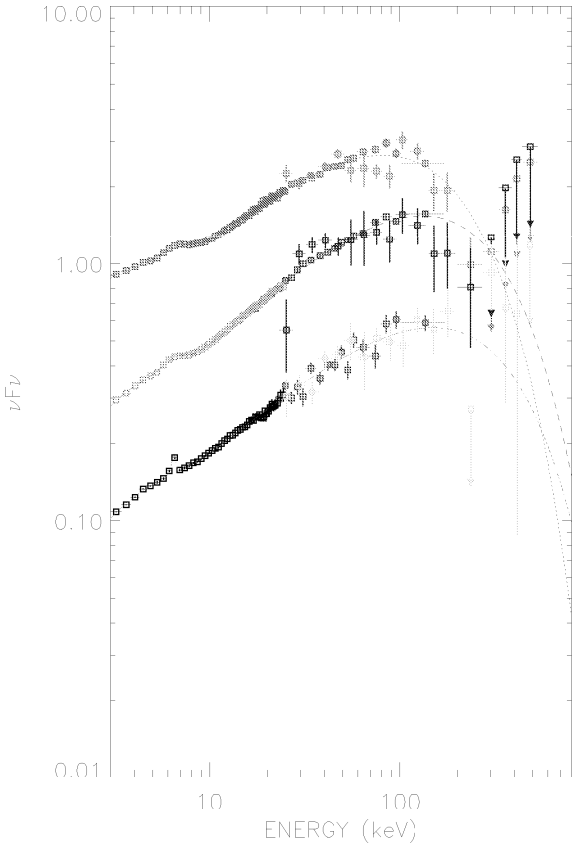

Fig. 2.— Spectra of GRO J1655−40 from PCA, SPI and HEXTE data fitted simultaneously with the model described in Table 4. PCA data for revolutions 289 (black), 292(indigo), 293 (brown); HEXTE data for revolutions 289 (red), 292(violet), 293 (grey); SPI data for revolutions 289 (yellow), 292(blue), 293 (green).

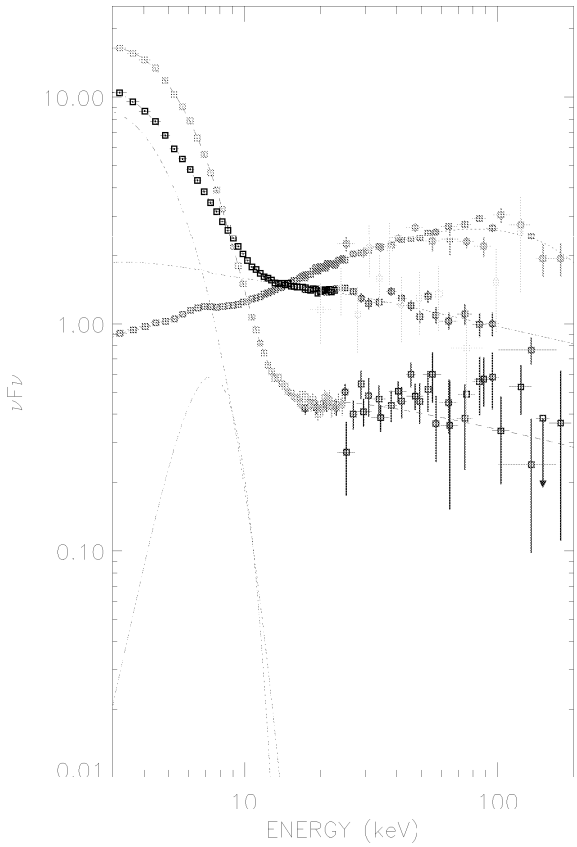

Fig. 3.— Spectra of GRO J1655−40 from PCA, SPI and HEXTE data fitted simultaneously with the model described in Table 4. PCA data for revolutions 293 (brown), 294-A (black), 295,6 (indigo); HEXTE data for revolutions 293 (gray), 294-A (red), 295,6 (violet); SPI data for revolutions 293 (green), 295,6 (blue) and BAT data for revolution 294_{sw}-B (yellow).

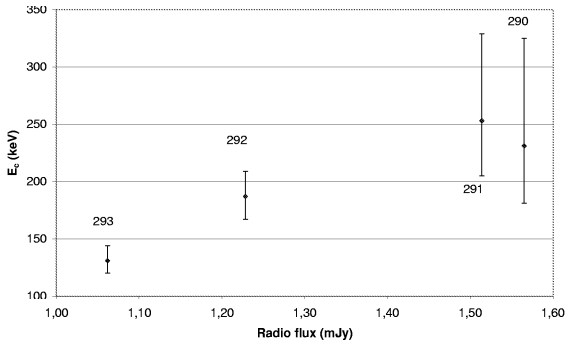

Fig. 4.— Evolution of the high energy cutoff (E_c expressed in keV) derived from the model given in Table 4, as a function of the radio flux measured by VLA at 8.460 GHz (Shaposhnikov et al. 2007). The INTEGRAL revolution numbers have been mentioned on the graph.

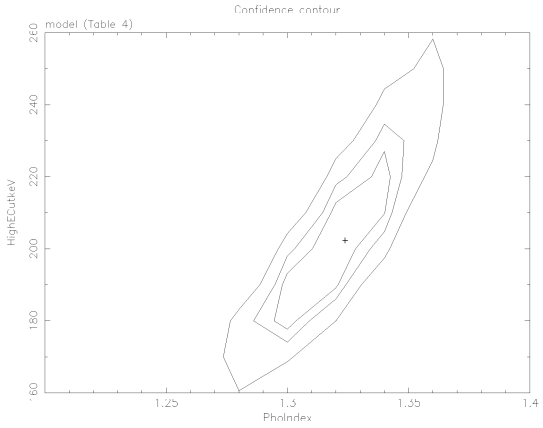

Fig. 5.— Γ-E_c contour plot for the simultaneous PCA, HEXTE, ISGRI and SPI observations using the model described in Table 4. The curves refer to $\delta\chi^2 = 2.30$, 4.61, 9.21, corresponding to confidence levels of 68, 90 and 99% for two interesting parameters.

Rev.	SP_{start}	SP_{stop}	Δt_{sp} (ks)	ID	RX_{start}	RX_{stop}	Exp.(ks)
289	53425.14	53427.36	133	90058-16-04-00	53425.06	53425.10	3.7
				90428-01-01-00	53426.04	53426.28	20.6
				90058-16-05-00	53427.02	53427.06	3.1
290	53428.13	53430.36	134	90428-01-01-03	53428.14	53428.20	5.1
				90428-01-01-04	53428.86	53429.12	22.5
				90428-01-01-02	53429.71	53429.97	22.6
290_{ibis} (A)	53428.20	53429.50	69				
291	53432.85	53433.47	29	90428-01-01-10	53432.79	53433.00	17.97
292	53434.80	53436.42	36	91404-01-01-02	53433.91	53434.09	16.14
				91404-01-01-03	53434.69	53434.73	2.80
				91404-01-01-01	53435.61	53435.64	2.37
				91404-01-01-04	53436.16	53436.17	1.41
292_{sw}-A,B	53434.89	53436.45	17.75				
293a	–	–	–	91702-01-01-00	53436.72	53436.81	7.4
293_{sw}	53436.48	53436.49	14.89				
293	53437.11	53438.34	51	91702-01-01-03	53438.05	53438.08	2.2
294a	–	–	–	91704-04-01-00	53439.61	53439.65	3.4
294b	–	–	–	91704-04-01-01	53439.74	53439.78	3.6
294_{sw}-A	53439.05	53439.65	13.29				
294-A	–	–	–	91702-01-02-00	53440.68	53440.77	7.6
294_{sw}-B	53440.72	53441.87	4.42				
294-B	–	–	–	91702-01-02-01	53441.51	53441.54	2.3
294-B	–	–	–	91702-01-02-02	53441.59	53441.60	1.4
294-B	–	–	–	91702-01-02-03	53441.98	53442.01	2.2
294-C	–	–	–	91702-01-02-04	53442.06	53442.07	1.8
294-C	–	–	–	91702-01-02-05	53442.12	53442.14	1.5
294-C	–	–	–	91702-01-02-06	53442.58	53442.66	6.9
295-A	–	–	–	91702-01-03-00	53443.54	53443.80	22.5
$295,6_{sw}$	53444.92	53447.21	15.33				
295,6	53445.07	53447.71	75	91702-01-04-01	53444.49	53444.50	0.6
$295,6_{ibis}(A)$	53445.10	53447.80	72				

Table 1: The INTEGRAL observations of GRO J1655-40. For each INTEGRAL revolution (Rev.), we give the beginning SP_{start} and the end SP_{stop} of the INTEGRAL observations in MJD from SPI detector. *(A) As the observation period was not the same for SPI and IBIS detectors, we indicate this first one for IBIS data (revolutions 290_{ibis}, $295,6_{ibis}$).* Δt_{sp} is the useful duration for INTEGRAL observations. ID is the identification program number of RXTE observations. RX_{start} and RX_{stop} are the beginning and the end of RXTE observations taken quasi simultaneously with INTEGRAL observations. Exp. is the exposure time for PCA. We indicate the simultaneous BAT data: the symbol "sw" is attached to the number of the revolution. The details of the BAT observations are given in Table 2. We separated with a line the observation period for which the source harboured the same X-ray state (see section 3.1 and Figure 1). This will be done for all Tables in this article.

Rev.	ID	Sw_{start}	Sw_{stop}	Exp(ks)
292_{sw}-A	00106709002	53434.89	53434.91	1.35
	00106709003	53435.23	53435.24	1.35
	00030009002	53435.42	53435.50	2.94
	00106709004	53435.76	53435.78	0.90
	00055750001	53436.08	53436.09	0.90
	00055750002	53436.15	53436.16	1.30
	00055750003	53436.21	53436.23	1.35
292_{sw}-B	00106709005	53436.23	53436.25	1.35
	00055750004	53436.28	53436.30	1.35
	00058739002	53436.30	53436.32	1.66
	00055750005	53436.35	53436.35	0.64
	00058739002	53436.37	53436.38	1.04
	00055750006	53436.41	53436.42	0.64
	00058739002	53436.44	53436.45	0.98
293_{sw}	00055750007	53436.48	53436.49	0.64
	00055750008	53436.54	53436.55	0.45
	00107547001	53436.62	53437.17	18.30
294_{sw}-A	00107547002	53439.05	53439.65	13.29
294_{sw}-B	00058736001	53440.72	53440.93	1.80
	00058746001	53440.98	53441.00	1.80
	00058746002	53441.07	53441.87	0.82
$295,6_{sw}$	00055800001	53444.92	53445.13	1.24
	00111063001	53446.14	53446.88	12.60
	00058752001	53447.06	53447.21	1.49

Table 2: Details about BAT data observations. We give the observation ID number, the beginning Sw_{start} and the end Sw_{stop} of the BAT observations in MJD. Exp is the net exposure time.

rev	Φ [23-51 keV]	Φ [51-95 keV]	Φ [95-160 keV]	Φ [160-270 keV]
289	42^{+2}_{-2}	64^{+6}_{-6}	81^{+7}_{-7}	59^{+16}_{-16}
290	49^{+4}_{-4}	74^{+9}_{-9}	89^{+7}_{-7}	87^{+21}_{-21}
291	50^{+14}_{-14}	116^{+30}_{-30}	88^{+30}_{-30}	167^{+70}_{-70}
292	125^{+8}_{-8}	159^{+19}_{-19}	245^{+25}_{-25}	187^{+50}_{-50}
293_{sw}	241^{+3}_{-4}	320^{+7}_{-6}	403^{+12}_{-12}	–
293	280^{+7}_{-7}	327^{+13}_{-13}	358^{+14}_{-14}	214^{+37}_{-37}
294_{sw}-A	328^{+5}_{-5}	357^{+7}_{-7}	382^{+14}_{-12}	–
294_{sw}-B	367^{+6}_{-7}	347^{+11}_{-10}	332^{+17}_{-17}	–
$295{,}6_{sw}$ (A)	81^{+3}_{-3}	76^{+6}_{-6}	73^{+10}_{-9}	-

Table 3: Flux Φ (expressed in mCrab) of GRO J1655-40 measured by SPI during different INTEGRAL revolutions (rev) and for several energy bands. (a) The data from the revotion 295 and 296 have been merged.

rev	T_{in} keV	N_{in}	Γ	E_c keV	W_{Fe} eV	χ^2(dof)	F-test	ϕ_p/ϕ
289	$1.29^{+0.12}_{-0.12}$	$0.80^{+0.37}_{-0.23}$	$1.47^{+0.02}_{-0.02}$	—	76^{+67}_{-60}	1.86 (79)		
289	$1.41^{+0.08}_{-0.14}$	$1.41^{+0.49}_{-0.17}$	$1.36^{+0.04}_{-0.04}$	231^{+94}_{-50}	75^{+42}_{-48}	0.95(78)	3.62E-10	9.6
290	$1.20^{+0.10}_{-0.05}$	$1.05^{+0.58}_{-0.31}$	$1.47^{+0.01}_{-0.01}$	—	75^{+36}_{-50}	2.04(79)		
290	$1.40^{+0.08}_{-0.09}$	$1.21^{+0.33}_{-0.22}$	$1.33^{+0.03}_{-0.03}$	259^{+62}_{-41}	76^{+42}_{-40}	0.86(78)	1.85E-16	9.6
290 (C)	$1.09^{+0.12}_{-0.11}$	$1.15^{+0.73}_{-0.44}$	$1.51^{+0.01}_{-0.01}$	—	69^{+41}_{-41}	3.45(108)		
290 (C)	$1.39^{+0.07}_{-0.08}$	$1.32^{+0.34}_{-0.23}$	$1.32^{+0.01}_{-0.03}$	200^{+29}_{-23}	77^{+58}_{-77}	1.37(107)	1.69E-23	9.7
291	$1.04^{+0.14}_{-0.15}$	$2.64^{+3.27}_{-1.15}$	$1.46^{+0.01}_{-0.01}$	—	75^{+36}_{-50}	1.60(79)		
291	$1.40^{+0.12}_{-0.16}$	$1.37^{+0.82}_{-0.32}$	$1.34^{+0.03}_{-0.04}$	253^{+76}_{-48}	78^{+42}_{-42}	0.85(78)	1.42E-12	8.7
292	$1.09^{+0.08}_{-0.08}$	$4.32^{+1.87}_{-1.24}$	$1.48^{+0.01}_{-0.01}$	—	113^{+72}_{-82}	4.48(77)		
292	$1.27^{+0.09}_{-0.08}$	$4.49^{+1.42}_{-1.12}$	$1.29^{+0.02}_{-0.02}$	187^{+22}_{-20}	177^{+88}_{-81}	0.85(76)	2.27E-29	7.5
292 + 292_{sw}	$1.27^{+0.09}_{-0.08}$	$4.50^{+1.42}_{-1.12}$	$1.29^{+0.02}_{-0.02}$	186^{+22}_{-18}	76^{+42}_{-40}	0.68(223)		
293_{sw} + 293a	$0.93^{+0.06}_{-0.06}$	22^{+9}_{-6}	$1.53^{+0.01}_{-0.01}$	–	145^{+75}_{-52}	3.85(118)	–	–
293_{sw} + 293a	$1.07^{+0.05}_{-0.05}$	22^{+5}_{-4}	$1.33^{+0.02}_{-0.02}$	173^{+21}_{-17}	315^{+93}_{-57}	1.35(117)	1.19E-28	7.4
293	$1.60^{+0.05}_{-0.01}$	$4.87^{+1.52}_{-0.76}$	$1.62^{+0.05}_{-0.05}$	—	388^{+46}_{-39}	5.30(77)		
293	$1.00^{+0.03}_{-0.03}$	45^{+21}_{-15}	$1.37^{+0.02}_{-0.03}$	131^{+13}_{-11}	386^{+80}_{-52}	1.15(76)	3.46E-27	5.3
294_{sw}-A + 294a,b	$0.67^{+0.03}_{-0.03}$	286^{+17}_{-14}	$1.82^{+0.3}_{-0.02}$	–	166^{+28}_{-38}	14.32(118)	–	
294_{sw}-A + 294a,b	$1.01^{+0.03}_{-0.03}$	121^{+17}_{-14}	$1.41^{+0.3}_{-0.02}$	87^{+4}_{-5}	646^{+67}_{-46}	1.37(117)	–	4.4
294-B+294_{sw}-B	$0.98^{+0.01}_{-0.01}$	1681^{+64}_{-66}	$2.18^{+0.01}_{-0.02}$	–	622^{+35}_{-44}	1.16(118)		
294-B+294_{sw}-B	$0.98^{+0.01}_{-0.01}$	1687^{+65}_{-61}	$2.08^{+0.05}_{-0.04}$	302^{+225}_{-81}	673^{+50}_{-41}	0.99(117)	1.682E-05	0.41
294-C	$1.02^{+0.01}_{-0.01}$	1686^{+54}_{-67}	$2.15^{+0.01}_{-0.01}$	–	522^{+174}_{-108}	1.96(62)		
294-C	$1.02^{+0.01}_{-0.01}$	1676^{+61}_{-57}	$2.08^{+0.02}_{-0.04}$	439^{+418}_{-153}	538^{+35}_{-49}	1.81(61)	1.49E-02	0.29
295-A	$1.09^{+0.01}_{-0.01}$	1709^{+60}_{-47}	$2.02^{+0.01}_{-0.01}$	> 800	340^{+38}_{-37}	1.40(62)		0.15
295-B+295_{sw}	$1.15^{+0.01}_{-0.01}$	1454^{+63}_{-29}	$1.85^{+0.07}_{-0.05}$	> 261	103^{+50}_{-50}	1.03(135)		0.05
295-B+295_{sw}	$1.15^{+0.01}_{-0.01}$	1464^{+37}_{-27}	$1.87^{+0.04}_{-0.05}$	—	110^{+91}_{-80}	1.02(136)		0.05
295,6+295,6_{sw}	$1.13^{+0.01}_{-0.01}$	1760^{+20}_{-9}	$2.17^{+0.01}_{-0.01}$	—	188^{+52}_{-43}	0.86(167)		0.07
295,6+295,6_{sw}	$1.14^{+0.01}_{-0.01}$	1649^{+231}_{-134}	$2.05^{+0.11}_{-0.07}$	> 237	167^{+46}_{-44}	0.84(166)		0.05

Table 4: PCA, SPI and HEXTE data fitted simultaneously using the XSPEC multicomponent model PHABS*(GAUSSIAN+DISKBB+POWERLAW). T_{in} is the inner disk temperature and N_{in} the normalisation, a Gaussian line was fixed at an energy of 6.4 keV with a width fixed to 0.1 keV for rev 289, 290. W_{Fe} is the equivalent width. The interstellar absorption PHABS has been fixed to 0.7×10^{22} cm^{-2} until the dataset 294-A and to 0.5×10^{22} cm^{-2} from the revolution 294-B onward. Γ is the photon index. The POWERLAW component was replaced by a CUTOFFPL component and E_c is the high energy cut-off. The F-test is calculated between the POWERLAW and CUTOFFPL models. We also give the ratio ϕ_p/ϕ_b where ϕ_p and ϕ_b are the powerlaw and the blackbody flux in the 2-20 keV energy range respectively. χ^2(dof) is the reduced χ^2 with the degree of freedom (dof). For revolution 290 (c) as well as for revolutions 295 and 296 which have been combined, the ISGRI data have been added.

rev	Γ	E_c keV	T_{in} keV	N_{in}	W_{Fe} eV	χ^2(dof)	$L_{3-600} \times 10^{-9}$ ergs cm^{-2} s^{-1}
289	$1.36^{+0.04}_{-0.08}$	237^{+143}_{-55}	$1.38^{+0.12}_{-0.11}$	$1.07^{+0.48}_{-0.27}$	80^{+65}_{-78}	0.98(77)	$2.9^{+0.1}_{-0.1}$
290	$1.33^{+0.01}_{-0.06}$	255^{+108}_{-35}	$1.44^{+0.05}_{-0.11}$	$1.07^{+0.26}_{-0.15}$	71^{+55}_{-61}	0.89(77)	$3.5^{+0.1}_{-0.1}$
290 (C)	$1.33^{+0.08}_{-0.01}$	207^{+111}_{-16}	$1.32^{+0.04}_{-0.01}$	$1.68^{+0.56}_{-0.51}$	86^{+62}_{-78}	1.40(106)	$3.3^{+0.02}_{-0.2}$
291	$1.37^{+0.10}_{-0.02}$	316^{+232}_{-23}	$1.36^{+0.17}_{-0.26}$	$2.36^{+3.81}_{-0.90}$	< 130	0.85(77)	$6.4^{+0.5}_{-0.6}$
292	$1.29^{+0.03}_{-0.02}$	185^{+30}_{-19}	$1.27^{+0.10}_{-0.08}$	$5.73^{+1.80}_{-1.43}$	< 173	0.93(77)	$8.1^{+0.4}_{-0.1}$
293_{sw} + 293a	$1.33^{+0.07}_{-0.02}$	171^{+59}_{-15}	$1.07^{+0.05}_{-0.05}$	22^{+5}_{-4}	317^{+80}_{-50}	1.36(116)	$10.6^{+0.6}_{-0.3}$
293	$1.37^{+0.05}_{-0.05}$	131^{+14}_{-8}	$1.04^{+0.06}_{-0.04}$	48^{+18}_{-16}	381^{+88}_{-82}	1.22(77)	$13.9^{+0.5}_{-0.1}$
294_{sw}-A + 294a,b	$1.42^{+0.05}_{-0.05}$	88^{+14}_{-8}	$1.00^{+0.06}_{-0.04}$	121^{+18}_{-16}	645^{+59}_{-56}	1.39(16)	$15.35^{+0.1}_{-0.1}$
294-B+294_{sw}-B	$2.07^{+0.12}_{-0.01}$	289^{+151}_{-36}	$0.97^{+0.01}_{-0.01}$	1752^{+24}_{-86}	701^{+100}_{-75}	1.06(116)	$18.13^{+0.03}_{-0.03}$
295-A	$2.03^{+0.05}_{-0.01}$	> 700	$1.09^{+0.01}_{-0.01}$	1709^{+55}_{-56}	> 156	1.45(60)	$23.39^{+0.25}_{-0.16}$
295-B+295_{sw}-B	$1.86^{+0.04}_{-0.12}$	> 457	$1.15^{+0.01}_{-0.01}$	1457^{+64}_{-32}	110^{+60}_{-61}	1.03(134)	$22.19^{+0.32}_{-0.11}$
295,6+$295,6_{sw}$ (C)	$2.16^{+0.04}_{-0.11}$	> 2000	$1.14^{+0.01}_{-0.01}$	1509^{+67}_{-58}	< 840	0.82(164)	$20.84^{+3.24}_{-1.72}$

Table 5: PCA, HEXTE and SPI data fitted simultaneously using the XSPEC multicomponent model PHABS*(PEXRAV+GAUSSIAN+DISKBB). Γ is the photon index and E_c the energy cut-off. T_{in} is the inner disk temperature and N_{in} the normalisation. The interstellar absorption PHABS has been fixed to 0.7×10^{22} cm^{-2} until the dataset 294-A and to 0.5×10^{22} cm^{-2} from the revolution 294-B onward. The Gaussian line was fixed at an energy of 6.4 keV. W_{Fe} is the equivalent width. the reflection fraction $\Omega/2\pi$ has been found with an upper value ranging 0.1-0.2. L_{3-600} is the luminosity of the source in the 3-600 keV energy range. χ^2(dof) is the reduced χ^2 with the degree of freedom (dof). (c) The ISGRI data have been included.

rev	kT keV	τ	T_{in} keV	N_{in}	χ^2(dof)	y
289	43^{+16}_{-8}	$1.78^{+0.26}_{-0.37}$	$0.83^{+0.04}_{-0.04}$	12^{+3}_{-2}	1.04(79)	$1.07^{+0.40}_{-0.23}$
290	40^{+6}_{-4}	$1.92^{+0.13}_{-0.14}$	$0.80^{+0.03}_{-0.03}$	16^{+3}_{-2}	0.93(78)	$1.15^{+0.17}_{-0.12}$
290 (C)	36^{+4}_{-3}	$1.98^{+0.14}_{-0.12}$	$0.76^{+0.01}_{-0.03}$	18^{+}_{-}	1.82(106)	$1.12^{+0.12}_{-0.10}$
291	36^{+12}_{-6}	$2.07^{+0.15}_{-0.17}$	$0.78^{+0.07}_{-0.06}$	34^{+10}_{-21}	0.84(77)	$1.21^{+0.40}_{-0.21}$
292	35^{+2}_{-2}	$2.09^{+0.10}_{-0.07}$	$0.80^{+0.02}_{-0.04}$	44^{+10}_{-4}	1.36(77)	$1.20^{+0.07}_{-0.07}$
293_{sw} + 293a	31^{+2}_{-1}	$2.15^{+0.1}_{-0.1}$	$0.77^{+0.02}_{-0.02}$	106^{+16}_{-13}	1.63(117)	$1.12^{+0.07}_{-0.08}$
293	31^{+2}_{-2}	$2.01^{+0.09}_{-0.09}$	$0.74^{+0.10}_{-0.12}$	244^{+338}_{-93}	1.31(77)	$0.98^{+0.06}_{-0.06}$
294_{sw}-A + 294a,b	26^{+2}_{-2}	$1.93^{+0.09}_{-0.09}$	$0.76^{+0.10}_{-0.12}$	457^{+338}_{-93}	2.06(117)	$0.76^{+0.06}_{-0.06}$
294-B+294_{sw}-B	282^{+38}_{-41}	$0.03^{+0.01}_{-0.01}$	$0.95^{+0.01}_{-0.01}$	2065^{+51}_{-115}	1.07(117)	$0.06^{+0.01}_{-0.01}$
294-B+294_{sw}-B (A)	59^{+33}_{-23}	$0.55^{+0.38}_{-0.21}$	$0.95^{+0.03}_{-0.02}$	1183^{+200}_{-221}	0.75(115)	$0.25^{+0.14}_{-0.14}$
294-C	320^{+54}_{-92}	$0.02^{+0.02}_{-0.01}$	$1.00^{+0.01}_{-0.01}$	1967^{+75}_{-58}	1.91(61)	$0.05^{+0.01}_{-0.03}$
294-C (A)	86^{+61}_{-38}	$0.43^{+0.51}_{-0.23}$	$1.06^{+0.03}_{-0.03}$	1192^{+197}_{-172}	1.26(59)	< 0.20
295-B+295_{sw}-B	763^{+161}_{-610}	< 0.07	$1.24^{+0.01}_{-0.01}$	1267^{+52}_{-37}	1.02(135)	< 0.06
295,6+$295,6_{sw}$ (C)	445^{+348}_{-88}	< 0.12	$1.17^{+0.01}_{-0.01}$	1402^{+63}_{-48}	1.04(165)	< 0.07

Table 6: PCA, HEXTE and SPI data fitted simultaneously using the XSPEC multicomponent model PHABS*(COMPTT+GAUSSIAN+DISKBB). The interstellar absorption PHABS has been fixed to 0.7×10^{22} cm^{-2} until the dataset 294-A and to 0.5×10^{22} cm^{-2} from the revolution 294-B onward. T_{in} is the inner disk temperature, N_{in} the normalisation, τ the optical depth and kT the plasma temperature. The Compton parameter y (see the definition in the text) has been determined. (a) For the dataset 294-B and 294-C a powerlaw component Γ of $3.86^{+0.12}_{-0.18}$ and $3.95^{+0.40}_{-0.35}$ was added, respectivelly. χ^2(dof) is the reduced χ^2 with the degree of freedom (dof). (c) The simultaneous ISGRI data have been taken into account.